

Absorption-dispersion in a three-level electromagnetically induced transparency medium including near dipole-dipole interaction effects

Amitabh Joshi*

Department of Physics and Optical Engineering, Rose-Hulman Institute of Technology, Terre Haute, Indiana 47803, USA

Juan D. Serna**

Department of Physics and Electrical Engineering, University of Scranton, Scranton, Pennsylvania 18510, USA

Abstract

Dynamical evolution and electromagnetically induced transparency (EIT) is investigated here in a three-level λ -type atomic system including near-dipole-dipole interaction among atoms. The system is driven by the probe and coupling fields. Exact numerical solutions under steady-state condition are given for the density operator equation to get information about population in various levels and the linear susceptibility of probe-transition. Also, obtained are the closed form expressions for linear and third order non-linear susceptibilities for the probe transition under perturbation approximation.

Keywords: Electromagnetically induced transparency, near dipole-dipole interactions, three-level atom, strong atom-field coupling

PACS: 42.50.Ct; 42.50.Gy

1. Introduction

It has been shown in the late eighties that the propagation of an electromagnetic field with a medium composed of two-level atoms can generate near dipole-dipole (NDD) interaction. Such NDD effects can result in the inversion-dependent-chirping of the single atom resonance frequency of such two-level atomic dipole system. The NDD interactions give rise to a local effect that modifies the microscopic field coupling the atom and which

*Principal corresponding author

**Corresponding author

Email addresses: mcbamji@gmail.com (Amitabh Joshi), juan.serna@scranton.edu (Juan D. Serna)

Preprint submitted to Elsevier

May 25, 2018

is obtained from the macroscopic field and the induced polarization [1]. The significant contribution of the NDD interaction comes from the entities enclosed in a tiny volume of the order of a cubic wavelength, and that is prominent in a dense medium. The use of the modified Maxwell-Bloch equation allowed to predict many interesting results caused by NDD effects. For example, invariant pulse propagation that departs from the hyperbolic secant pulse shape (with pulse area different from 2π) related to self-induced transparency (SIT) [2] and self-phase modulation in SIT [3]. Other relevant results include the observation of intrinsic optical bistability (IOB) when the atomic number density and the oscillator strengths are very high [4]; enhancement of gain in systems showing inversionless lasing; optical switching; among others. When a sample of atoms interacts with the external driving field, then the generated reaction field due to the induced dipoles in this samples works against the applied field leading to a decrease in the net field. If the external driving field is stronger than the generated reaction field due to the dipole-dipole interaction, then the manifestation of the suppression of reaction field can be observed as a first-order phase transition far away from the equilibrium condition [5, 6].

Modified nonlinear Maxwell-Bloch equations are required to describe the interaction of the propagating electromagnetic field in a dense two-level medium [1]. In an optically dense medium, the near dipole-dipole interaction among atoms (occurring at microscopic scale) plays a significant role and leads to the renormalization of the resonance frequency of transition. This renormalization is governed by the population inversion in the two-level system. However, to get a relationship between the macroscopic electric field \mathbf{E}_M and the polarization \mathbf{P} to the microscopic field \mathbf{E}_m (causing the excitation in the atomic system through the dipole interaction), the Lorentz-Lorentz relation

$$\mathbf{E}_m = \mathbf{E}_M + \frac{4\pi}{3} \mathbf{P} \quad (1)$$

is required. This equation is valid for homogeneous and isotropic media of the static fields. According to the extinction theorem [7], such an equation is also valid for the monochromatic time-dependent propagating field in a linear, homogeneous, and isotropic medium. However, in an optically dense medium where many interesting nonlinear effects can be studied, one needs to get a proper relationship between the microscopic and the macroscopic fields.

Maxwell's equations along with Eq. (1) (related to the local field correction) provide a Clausius-Mossotti relation between the microscopic polarizability β , and the macroscopic dielectric parameter ϵ_M , of any solid, liquid or gaseous medium. This relation takes the form [1]

$$\beta = \frac{3}{4\pi N} \left(\frac{\epsilon_M - 1}{\epsilon_M + 2} \right), \quad (2)$$

where N is the number of entities (atoms or molecules) per unit volume. Causality and retardation phenomena are essential to explain the propagation of time-dependent fields. In the literature, it has been shown using the extinction theorem that for a linear, homogeneous, and isotropic medium, Eq. (1) works well and hence Eq. (2) is also appropriate for such medium [1]. The propagation of a field in a dense and nonlinear medium consisting of multi-level atoms requires modified atomic and field equations to include the effect of induced dipole-dipole interaction in these equations.

The Maxwell's wave equation provides the relationship between the macroscopic electric field \mathbf{E}_M , and the macroscopic polarization \mathbf{P}

$$\nabla^2 \mathbf{E}_M - \frac{1}{c^2} \frac{\partial^2 \mathbf{E}_M}{\partial t^2} = \frac{4\pi}{c^2} \frac{\partial^2 \mathbf{P}}{\partial t^2}, \quad (3)$$

with c the speed of light in vacuum. The vector quantities \mathbf{E}_M and \mathbf{P} are waves traveling in the z -direction and expressed as

$$\begin{aligned} \mathbf{E}_M &= \varepsilon e^{-i(\omega t - k_z z)} + c.c. \\ \mathbf{P} &= \wp e^{-i(\omega t - k_z z)} + c.c. \end{aligned} \quad (4)$$

with wave vector k_z , frequency ω , and slowly varying quantities ε and $\wp = i\mu N D_{ab}$. N is the density of two-level atoms in the medium and μ is the transition dipole matrix element.

In general, the microscopic field interacting with the atomic dipole is not identical with the macroscopic field appearing in Maxwell's equations. This difference is because the field driving the atom does not contain the local field of the atom. On the other hand, the macroscopic field of Maxwell's equations does include the local field. Hence, it is essential to get a relationship between the microscopic and macroscopic field when the atomic system is optically dense (which means a large number of atoms within a cubic resonance wavelength) [1].

In previous works [1, 6] for the two-level system, the Maxwell-Bloch equations for the dense medium under the slowly-varying-envelope approximation for the field were obtained for a homogeneous medium that contained a large number of atoms within a small volume determined by the cube of the resonance wavelength. In earlier work [8], the effects of near dipole-dipole interaction on a three-level system undergoing lasing without inversion were studied, and enhancements in inversionless gain and refractive index without absorption were predicted. However, in that work, the authors treated the problem differently from the way we intend to show in this present work on a three-level system. In another work, the effect of dipole-dipole interaction has been discussed in the cavity quantum electrodynamics of two-level atoms [9, 10].

This paper is organized as follows: Section 2 describes the model under consideration followed by some analytical results for linear and third-order susceptibilities of the probe transition in Section 3. Numerical results for absorption and dispersion are discussed in Section 4 by solving the exact density matrix equation. In Section 5 some concluding remarks are provided.

2. The model

In this work, we extend the development of atomic density operator equations for a three-level atomic system when the fields are propagating in an optically dense medium. Such a dense medium is characterized by a high number of atoms within the volume determined by the cube of the resonance wavelength. The medium consists of a three-level

system in a λ -type configuration of its levels [11, 12]. The model under consideration uses a semiclassical approximation where the system interacts with the classical electromagnetic fields of two lasers. The probe and coupling laser beams with frequencies ω_P and ω_C , respectively, interact with the atomic transitions ω_{21} and ω_{23} , as shown in Fig. 1. The Liouville equations of density-matrix elements in the dipole and rotating wave approximations are given by [11, 12]

$$\begin{aligned}
\dot{\rho}_{22} - \dot{\rho}_{11} &= -(\gamma_{23} + 2\gamma_{21})\rho_{22} + 2i\mu_{12}(\varepsilon_L^P)^* \rho_{21} - 2i\mu_{12}(\varepsilon_L^P)\rho_{12} \\
&\quad + i\mu_{23}(\varepsilon_L^C)^* \rho_{23} - i\mu_{23}(\varepsilon_L^C)\rho_{32} - \gamma_{31}(\rho_{33} - \rho_{11}), \\
\dot{\rho}_{22} - \dot{\rho}_{33} &= -(2\gamma_{23} + \gamma_{21})\rho_{22} + i\mu_{12}(\varepsilon_L^P)^* \rho_{21} - i\mu_{12}(\varepsilon_L^P)\rho_{12} \\
&\quad + 2i\mu_{23}(\varepsilon_L^C)^* \rho_{23} - 2i\mu_{23}(\varepsilon_L^C)\rho_{32} - \gamma_{31}(\rho_{11} - \rho_{33}), \\
\dot{\rho}_{23} &= -(\gamma + i\Delta_C)\rho_{23} + i\mu_{23}(\varepsilon_L^C)(\rho_{22} - \rho_{33}) - i\mu_{12}(\varepsilon_L^P)\rho_{13}, \\
\dot{\rho}_{21} &= -(\gamma + i\Delta_P)\rho_{21} + i\mu_{12}(\varepsilon_L^P)(\rho_{22} - \rho_{11}) - i\mu_{23}(\varepsilon_L^C)\rho_{31}, \\
\dot{\rho}_{31} &= -[\gamma_{31} + i(\Delta_P - \Delta_C)]\rho_{31} - i\mu_{23}(\varepsilon_L^C)^* \rho_{21} + i\mu_{12}(\varepsilon_L^P)\rho_{32}.
\end{aligned} \tag{5}$$

In Eq. (5), ε_L^P and ε_L^C are complex, microscopic, slowly-varying electric field envelopes of the probe and coupling fields, respectively. The radiative decay rates from levels $|2\rangle$ to $|1\rangle$ and $|2\rangle$ to $|3\rangle$ are γ_{21} and γ_{23} , respectively. The non-radiative decay rate between levels $|3\rangle$ and $|1\rangle$ is γ_{31} . We also introduce $\gamma = \frac{1}{2}(\gamma_{21} + \gamma_{32} + \gamma_{31})$. The Rabi frequencies of the probe and coupling fields are defined as $\Omega^P = 2\mu_{12}\varepsilon_L^P$ and $\Omega^C = 2\mu_{32}\varepsilon_L^C$, respectively. The transition dipole matrix elements for transitions between levels $|1\rangle$ and $|2\rangle$ ($|3\rangle$) is μ_{12} (μ_{23}), which will be commonly represented by the symbol μ_i (with $i = 12, 23$) in the subsequent discussion.

Since we have two electromagnetic fields interacting with the three-level system, we denote these microscopic fields by \mathbf{E}_L^i , with $i = P, C$, and P and C denoting the probe and coupling field, respectively. We consider fields to be linearly polarized and moving as plane waves. The three-level atom is stationary and located at position \mathbf{r}_l . The microscopic field is the sum of the external driving field and the reaction field of the induced dipoles in the medium [1]

$$\mathbf{E}_L^i(\mathbf{r}_l, t) = \mathbf{E}_{ext}^i(\mathbf{r}_l, t) + \sum_{m=1}^N \aleph_{lm}^i \exp[-i\mathbf{k}^i \cdot (\mathbf{r}_l - \mathbf{r}_m)] \rho^i(t - r_{rl}/c), \quad (t = P, C). \tag{6}$$

In Eq. (6), $\rho^P = \rho_{12}$ and $\rho^C = \rho_{23}$, and the quantity \aleph_{lm}^i is given by

$$\begin{aligned}
\aleph_{lm}^i &= (3/2)\zeta^i \left\{ \left[\frac{\mathbf{p}_l^i}{|\mathbf{p}_l^i|} \cdot \frac{\mathbf{p}_m^i}{|\mathbf{p}_m^i|} - \left(\frac{\mathbf{p}_l^i}{|\mathbf{p}_l^i|} \cdot \frac{\mathbf{r}_{lm}}{|\mathbf{r}_{lm}|} \right) \left(\frac{\mathbf{p}_m^i}{|\mathbf{p}_m^i|} \cdot \frac{\mathbf{r}_{lm}}{|\mathbf{r}_{lm}|} \right) \right] Q_1^i(kr_{lm}) \right. \\
&\quad \left. + \left(\frac{\mathbf{p}_l^i}{|\mathbf{p}_l^i|} \cdot \frac{\mathbf{r}_{lm}}{|\mathbf{r}_{lm}|} \right) \left(\frac{\mathbf{p}_m^i}{|\mathbf{p}_m^i|} \cdot \frac{\mathbf{r}_{lm}}{|\mathbf{r}_{lm}|} \right) Q_2^i(kr_{lm}) \right\},
\end{aligned} \tag{7}$$

with

$$\begin{aligned}
Q_1^i(kr_{lm}) &= ie^{ik^i r_{lm}} \left[\frac{1}{(k^i)^3 r_{lm}^3} - \frac{1}{k^i r_{lm}} + \frac{i}{(k^i)^2 r_{lm}^2} \right], \\
Q_2^i(k^i r_{lm}) &= 2ie^{-k^i r_{lm}} \left[-\frac{1}{(k^i)^3 r_{lm}^3} + i\frac{1}{(k^i)^2 r_{lm}^2} \right], \\
\zeta^i &= \frac{2|\mu_i|^2 (k^i)^3}{3\hbar};
\end{aligned} \tag{8}$$

In addition, $k^i = \omega^i/c$, $\mathbf{r}_{lm} = \mathbf{r}_l - \mathbf{r}_m$, and \mathbf{p}_l^i ($i = P, C$) are the dipole moments of the probe and coupling transitions.

The microscopic field \mathbf{E}_L^i has contributions of the nearby region specified by the condition $r_{lm} \ll \lambda$, the intermediate region, when $r_{lm} = \lambda$, and the far-off region, when $r_{lm} \gg \lambda$. The near-field defined by the parameter $E_{ne}^i(\mathbf{r}_l, t)$ is due to the atomic dipoles contained in a slab of thickness Δz around the position of the atom, situated at r_l . This field is a sort of microscopic contribution so that the other fields can be clubbed as the macroscopic field [1]. The field $E_{ne}^i(\mathbf{r}_l, t)$ gives non-zero contribution under the plane wave propagation condition in a homogeneous isotropic medium. In the following, we provide the estimates of these fields in different regions for the three-level system under consideration, just for the sake of completeness on the lines of Ref. [1], where a two-level medium was considered.

2.1. Microscopic Field in Nearby region

We estimate the microscopic fields by confining the atomic sample in a cylindrical shape geometry with the cylindrical axis along the z -direction. To make calculations simple, we assume the electromagnetic field as a plane wave propagating along the positive z -direction and the atomic location r_l on the z -axis. We also consider the dipoles of the medium to be pointing in the x -direction and plane polarized. Our goal is to estimate the field produced by all such identical dipoles (within a cylinder of diameter d) at location r_l . To evaluate the microscopic field, we replace the summation in Eq. (6) by an integral under the continuum limit to obtain [1]

$$E_{ne}^i(z, t) = \rho^i G^i(r, z, s) = (3/2)\rho^i \zeta^i N \int_0^{2\pi} d\theta \int_{-d/2}^{d/2} dz \int_{s_m}^{s_M} s ds H^i, \tag{9}$$

with

$$H^i = Q_1^i(k^i r) \sin^2 \theta + Q_2^i(k^i r) \cos^2 \theta + \frac{|z - z_l|^2}{r^2} [Q_1^i(k^i r) - Q_2^i(k^i r)] \cos^2 \theta, \tag{10}$$

and $r = (s^2 + |z - z_l|^2)^{1/2}$. Here, ρ^i (with $i = P, C$) represents the density matrix elements ρ_{21} and ρ_{23} ; s_m and s_M are the minimum and maximum values of s . We neglect the contribution of a small volume about the atom and around $z = z_l$, the quantity r_{lm} is approaching to r and $d \ll s_M$ while carrying out the integration and get

$$\langle G^i \rangle = \frac{2i\pi N \zeta^i}{(k^i)^3} + \frac{3\pi N \zeta^i d}{(k^i)^2}, \quad \text{with } i = P, C. \tag{11}$$

Clearly, Eq. (11) is a complex quantity whose real part depends on the diameter of the cylinder, d , but the imaginary part is independent of it. After substituting the value of ζ^i in Eq. (11), we get

$$\langle G^i \rangle = \frac{4i\pi|\mu_i|^2 N}{3\hbar} + \frac{2\pi N|\mu_i|^2 dk^i}{\hbar} = \epsilon_i + 2\gamma_i^D. \quad (12)$$

In the limiting condition, $2\pi d/\lambda^i = k^i \ll 1$, the contribution from the second term in Eq. (12) is negligibly small and thus the contribution from near dipoles coming under the condition $\Delta z \rightarrow 0$. Hence

$$E_{ne}^i(z, t) = \frac{4\pi}{3} \wp^i, \quad \text{with } i = P, C. \quad (13)$$

2.2. Macroscopic Field in intermediate and far-off regions

We estimate the contributions from the remaining fields replacing the summation by an integration in Eq. (6) (see Ref. [1])

$$\mathbf{E}_M^i(\mathbf{r}, t) = \int d^3r' U^i(|\mathbf{r} - \mathbf{r}'|) \exp[-ik^i \cdot (\mathbf{r} - \mathbf{r}')] \rho^i(\mathbf{r}', t - |\mathbf{r} - \mathbf{r}'|/c). \quad (14)$$

Notice that in this integral the contribution due to the nearby region is excluded, i.e., the region inside the slab of length Δz at z is omitted. Since we are considering here the plane-wave approximation for the field, then

$$\rho^i(\mathbf{r}', t - |\mathbf{r} - \mathbf{r}'|/c) = \rho^i(z', t - |z - z'|/c), \quad \text{with } i = P, C. \quad (15)$$

Substituting Eq. (15) in Eq. (14), and assuming cylindrical geometry for the atomic sample, the field contribution can be expressed as

$$\begin{aligned} \mathbf{E}_M^i(z_l, t) = N \int_0^{z_l-d} \int_0^{2\pi} \int_0^{s_M} s U^i(|z_l - z'|, s, \theta) e^{-ik^i(z_l - z')} \\ \times \rho^i(z', t - |z_l - z'|/c) ds d\theta dz', \end{aligned} \quad (16)$$

where

$$\begin{aligned} U^i = (3/2)\zeta^i \left\{ Q_1^i(k^i r) \sin^2 \theta + Q_2^i(k^i r) \cos^2 \theta \right. \\ \left. + \frac{|z - z_l|^2}{r^2} [Q_1^i(k^i r) - Q_2^i(k^i r)] \cos \theta \right\}. \end{aligned} \quad (17)$$

Here, r is as defined after Eq. (10); Q_1^i and Q_2^i are given in Eq. (8), assuming $r_{lm} \rightarrow r$. After integrating over the variables θ and s , and using the parameter $r_M = (k^i)^2 s_M^2 + (k^i)^2 |z - z_l|^2$ with $i = P, C$, we get

$$\begin{aligned} \mathbf{E}_M^i(z_l, t) = \frac{3\pi\zeta^i N}{(k^i)^2} \int_0^{z_l-d} dz' \rho^i(z', t - |z_l - z'|/c) \\ - \frac{3\pi\zeta^i n}{2(k^i)^2} \int_0^{z_l-d} dz' e^{-ik^i(z_l - z')} \rho^i(z', t - |z_l - z'|/c) \\ \times e^{ir_M} \left[1 + i(k^i)^2 \frac{|z' - z_l|^2}{r_M^3} \right], \end{aligned} \quad (18)$$

In the limiting condition $k s_M \gg 1$, the second term in Eq. (18) is negligible giving

$$\mathbf{E}_M^i(z_l, t) = \frac{3\pi\zeta^i N}{(k^i)^2} \int_0^{z_l-d} dz' \rho^i(z', t - |z_l - z'|/c), \quad \text{with } i = P, C. \quad (19)$$

If we just want to estimate the contribution from the intermediate region, then we need the condition $\Delta z \rightarrow 0$ and $z_l = d$ in Eq. (19). Using this condition, we get the expression which is equal to the second term of Eq. (12). Also, under the condition, $d \rightarrow 0$ and $z_l \rightarrow z$ Eq. (19) provides an estimation of the macroscopic field for both far and intermediate regions as

$$\mathbf{E}_M^i(z_l, t) = \frac{3\pi\zeta^n}{(k^i)^2} \int_0^z dz' \rho^i(z', t - |z_l - z'|/c), \quad \text{with } i = P, C. \quad (20)$$

Clearly, the contribution to macroscopic field comes from the retarded dipoles, satisfying causality conditions.

We obtain Maxwell's equations in SVEA by substituting the proper partial derivatives with time and position coordinates in Eq. (20), leading to

$$\frac{\partial E_M^i}{\partial t} + c \frac{\partial E_M^i}{\partial z} = \frac{3\pi\zeta^i c \mu_i}{(k^i)^2} \rho^i. \quad (21)$$

Here, $\rho^P = \rho_{12}$ and $\rho^C = \rho_{23}$ are off-diagonal density matrix elements for probe and coupling transitions, respectively. Now, we can combine all fields including Eq. (13) to get the total field seen by the atom at a general location z as

$$E_L^i(z, t) = E_{ex}^i(z, t) + E_M^i(z, t) + \frac{4\pi}{3} \wp^i(z, t), \quad \text{with } i = P, C \quad (22)$$

in which the evolution of the macroscopic field is governed by Maxwell's equations. The expression obtained in Eq. (22) is incidentally identical to that of Lorentz-Lorentz corrections. However, the physical reasons behind these two expressions are quite different. We redefine the slowly varying envelopes in Eq. (5) in view of Eqs. (12) and (22), where contributions of the external driving field, macroscopic and atom's self-field have been taken care off and thus we rewrite Eq. (5) as

$$\begin{aligned} \dot{\rho}_{22} - \dot{\rho}_{11} &= -(\gamma_{23} + 2\gamma_{21})\rho_{22} + 2i\mu_{12}(\varepsilon_L^P)^* \rho_{21} - 2i\mu_{12}(\varepsilon_L^P)\rho_{12} \\ &\quad + i\mu_{23}(\varepsilon_L^C)^* \rho_{23} - i\mu_{23}(\varepsilon_L^C)\rho_{32} - \gamma_{31}(\rho_{33} - \rho_{11}) - \gamma_{21}^D |\rho_{21}|^2 \\ \dot{\rho}_{22} - \dot{\rho}_{33} &= -(2\gamma_{23} + \gamma_{21})\rho_{22} + i\mu_{12}(\varepsilon_L^P)^* \rho_{21} - i\mu_{12}(\varepsilon_L^P)\rho_{12} \\ &\quad + 2i\mu_{23}(\varepsilon_L^C)^* \rho_{23} - 2i\mu_{23}(\varepsilon_L^C)\rho_{32} - \gamma_{31}(\rho_{11} - \rho_{33}) - \gamma_{23}^D |\rho_{23}|^2 \\ \dot{\rho}_{23} &= -i[\Delta_C - \epsilon_c(\rho_{22} - \rho_{33})]\rho_{23} - [\gamma - (\gamma_{23}^D/2)(\rho_{22} - \rho_{33})]\rho_{23} \\ &\quad + i\mu_{23}(\varepsilon_L^C)(\rho_{22} - \rho_{33}) - i\mu_{12}(\varepsilon_L^P)\rho_{13} \\ \dot{\rho}_{21} &= -i[\Delta_P - \epsilon_p(\rho_{22} - \rho_{11})]\rho_{21} - [\gamma - (\gamma_{21}^D/2)(\rho_{22} - \rho_{11})]\rho_{21} \\ &\quad + i\mu_{12}(\varepsilon_L^P)(\rho_{22} - \rho_{11}) - i\mu_{23}(\varepsilon_L^C)\rho_{31} \\ \dot{\rho}_{31} &= -[\gamma_{31} + i(\Delta_P - \Delta_C)]\rho_{31} - i[\epsilon_p(\rho_{22} - \rho_{11}) - \epsilon_c(\rho_{22} - \rho_{33})]\rho_{31} \\ &\quad - i\mu_{23}(\varepsilon_L^C)^* \rho_{21} + i\mu_{12}(\varepsilon_L^P)\rho_{32} \end{aligned} \quad (23)$$

3. Analytical results under perturbative approximation

Next, we find out the steady-state solution of the above density matrix to get expressions of linear and nonlinear susceptibilities of probe transition. We follow the iterative approach for this purpose and represent a general density matrix element as $\rho_{ij} = \rho_{ij}^{(0)} + \rho_{ij}^{(1)} + \rho_{ij}^{(2)} + \dots$, such that the higher order component is calculated with the help of lower order components. We also assume that the coupling field is stronger than the probe field and initially for the zeroth order all the atomic population is in the ground state, e.g., $\rho_{11}^{(0)} \simeq 1$, $\rho_{22}^{(0)} \simeq 0$, and $\rho_{33}^{(0)} \simeq 0$. Under all such approximation, it is possible to show that

$$\rho_{32}^{(1)} = \frac{i\Omega_P^*/2}{\gamma_{\text{eff}} + i\Delta_c - i\epsilon_c(\rho_{22} - \rho_{33})^{(0)}} \rho_{31}^{(1)} \quad (24)$$

$$\begin{aligned} \rho_{31}^{(1)} = & - \frac{i\Omega_C^*/2}{\gamma_{31} - i(\Delta_p - \Delta_c) + i[\epsilon_p(\rho_{22} - \rho_{11})^{(0)} - \epsilon_c(\rho_{22} - \rho_{33})^{(0)}]} \\ & \times \left\{ 1 + \frac{|\Omega_P|^2/4}{\gamma_{31} - i(\Delta_p - \Delta_c) + i[\epsilon_p(\rho_{22} - \rho_{11})^{(0)} - \epsilon_c(\rho_{22} - \rho_{33})^{(0)}]} \right. \\ & \left. \times \frac{1}{\gamma_{\text{eff}} + i\Delta_c - i\epsilon_c(\rho_{22} - \rho_{33})^{(0)}} \right\}^{-1} \rho_{21}^{(1)} \end{aligned} \quad (25)$$

$$\begin{aligned} \rho_{21}^{(1)} = & \frac{(i\Omega_P)}{2} (\rho_{22} - \rho_{11})^{(0)} \left(\gamma_{\text{eff}} - i\Delta_P + i\epsilon_P(\rho_{22} - \rho_{11})^{(0)} \right. \\ & + \frac{|\Omega_C|^2/4}{\gamma_{31} - i(\Delta_P - \Delta_C) + i[\epsilon_P(\rho_{22} - \rho_{11})^{(0)} - \epsilon_C(\rho_{22} - \rho_{33})^{(0)}]} \\ & \times \left\{ 1 + \frac{|\Omega_P|^2/4}{\gamma_{31} - i(\Delta_p - \Delta_c) + i[\epsilon_p(\rho_{22} - \rho_{11})^{(0)} - \epsilon_c(\rho_{22} - \rho_{33})^{(0)}]} \right. \\ & \left. \left. \times \frac{1}{\gamma_{\text{eff}} + i\Delta_c - i\epsilon_c(\rho_{22} - \rho_{33})^{(0)}} \right\}^{-1} \right)^{-1} \\ = & \frac{(i\Omega_P/2)(\rho_{22} - \rho_{11})^{(0)}}{F} \end{aligned} \quad (26)$$

where we have defined Ω_P and Ω_C after Eq. (5) and

$$\gamma_{\text{eff}} = \gamma - \frac{\gamma_1^D}{2} (\rho_{22} - \rho_{11})^{(0)} \quad (27)$$

with

$$\begin{aligned}
F &= \gamma_{\text{eff}} - i\Delta_P + i\epsilon_p(\rho_{22} - \rho_{11})^{(0)} \\
&+ \frac{|\Omega_C|^2/4}{\gamma_{31} - i(\Delta_P - \Delta_C) + i[\epsilon_p(\rho_{22} - \rho_{11})^{(0)} - \epsilon_c(\rho_{22} - \rho_{33})^{(0)}]} \\
&\times \left\{ 1 + \frac{|\Omega_P|^2/4}{\gamma_{31} - i(\Delta_P - \Delta_C) + i[\epsilon_p(\rho_{22} - \rho_{11})^{(0)} - \epsilon_c(\rho_{22} - \rho_{33})^{(0)}]} \right. \\
&\quad \left. \times \frac{1}{\gamma_{\text{eff}} + i\Delta_c - i\epsilon_c(\rho_{22} - \rho_{33})^{(0)}} \right\}^{-1}
\end{aligned} \tag{28}$$

We obtain the third order component in ρ_{21} (i.e., $\rho_{21}^{(3)}$), after calculating $\rho_{22} - \rho_{11}$ to the second order [i.e., $(\rho_{22} - \rho_{11})^{(2)}$]. Thus

$$\begin{aligned}
(\rho_{22} - \rho_{11})^{(2)} &= \frac{2}{2\gamma_{\text{eff}} + \gamma_{21}} \left[i\Omega_P^* \rho_{21}^{(1)} - i\Omega_P \rho_{12}^{(1)} \right] + \frac{2}{2\gamma_{\text{eff}} + \gamma_{21}}, \\
&= \frac{2}{2\gamma_{\text{eff}} + \gamma_{21}} \left(\frac{1}{F} + \frac{1}{F^*} \right) \left[-|\Omega_P|^2 (\rho_{22} - \rho_{11})^{(0)} \right] + \frac{2\gamma_{31}}{2\gamma_{\text{eff}} + \gamma_{21}}
\end{aligned} \tag{29}$$

$$\begin{aligned}
\rho_{21}^{(3)} &= \frac{i\Omega_P}{2} \left\{ \frac{1}{\gamma_{\text{eff}} + \gamma_{21}} \left(\frac{1}{F} + \frac{1}{F^*} \right) \left[-|\Omega_P|^2 (\rho_{22} - \rho_{11})^{(0)} \right] + \frac{2\gamma_{31}}{2\gamma_{\text{eff}} + \gamma_{21}} \right\} \\
&\times \left(\gamma_{\text{eff}} - i\Delta_P + \frac{i\epsilon_P}{2\gamma_{\text{eff}} + \gamma_{21}} \left\{ \left(\frac{1}{F} + \frac{1}{F^*} \right) \left[-|\Omega_P|^2 (\rho_{22} - \rho_{11})^{(0)} \right] + 2\gamma_{31} \right\} \right) \\
&+ \frac{|\Omega_C|^2/4}{\gamma_{31} - i(\Delta_P - \Delta_C) + \frac{i\epsilon_P}{2\gamma_{\text{eff}} + \gamma_{21}} \left\{ \left(\frac{1}{F} + \frac{1}{F^*} \right) \left[-|\Omega_P|^2 (\rho_{22} - \rho_{11})^{(0)} \right] + 2\gamma_{31} \right\}} \right\}^{-1}
\end{aligned} \tag{30}$$

In getting these expressions, quantities like $\rho_{33}^{(2)}$ and so are disregarded. Then, and up to third order of accuracy, the expression of ρ_{21} reads as

$$\begin{aligned}
\rho_{21} &\simeq \rho_{21}^{(1)} + \rho_{21}^{(3)} \\
&= i\Omega_P (\rho_{22} - \rho_{11})^{(0)} \left\{ \frac{1}{F} + \left[\frac{-|\Omega_P|^2}{\gamma_{\text{eff}} + \gamma_{21}} \left(\frac{1}{F} + \frac{1}{F^*} \right) + \frac{2\gamma_{31}}{2\gamma_{\text{eff}} + \gamma_{21}} \right] \right. \\
&\quad \times \left(\gamma_{\text{eff}} - i\Delta_P + \frac{i\epsilon_P}{2\gamma_{\text{eff}} + \gamma_{21}} \left\{ \left(\frac{1}{F} + \frac{1}{F^*} \right) \left[-|\Omega_P|^2 (\rho_{22} - \rho_{11})^{(0)} \right] + 2\gamma_{31} \right\} \right) \\
&\quad \left. + \frac{|\Omega_C|^2/4}{\gamma_{31} - i(\Delta_P - \Delta_C) + \frac{i\epsilon_P}{2\gamma_{\text{eff}} + \gamma_{21}} \left\{ \left(\frac{1}{F} + \frac{1}{F^*} \right) \left[-|\Omega_P|^2 (\rho_{22} - \rho_{11})^{(0)} \right] + 2\gamma_{31} \right\}} \right\}^{-1}
\end{aligned} \tag{31}$$

The macroscopic polarization of the atomic medium on the probe transition can be expressed as

$$P(M)_P = n \left(\rho_{12} \mu_{12} e^{-i\omega_P t} + \rho_{12}^* \mu_{12}^* e^{i\omega_P t} \right). \tag{32}$$

Alternatively, the macroscopic polarization can also be written as

$$P(M)_P = (1/2)\epsilon_0 (E_P\chi e^{-i\omega_P t} + E_P^*\chi^* e^{i\omega_P t}), \quad (33)$$

where χ is the electrical susceptibility of the medium on the probe transition. With the help of Eqs. (32) and (33), we get

$$\chi = \frac{2n\mu_{12}\rho_{12}}{\epsilon_0 E_P}, \quad (34)$$

such that

$$\chi = \chi^{(1)} + 3|E_P|^2\chi^{(3)}. \quad (35)$$

Then, we can write expressions for the first- and third-order susceptibilities as

$$\chi^{(1)} = i \frac{n|\mu_{12}|^2}{\epsilon_0 \hbar} \left[\frac{(\rho_{22} - \rho_{11})^{(0)}}{F} + \frac{2\gamma_{31}}{(2\gamma_{\text{eff}} + \gamma_{21})K} \right], \quad (36)$$

$$\chi^{(3)} = -i \frac{n|\mu_{12}|^4(\rho_{22} - \rho_{11})^{(0)}}{3\epsilon_0 \hbar^3(2\gamma_{\text{eff}} + \gamma_{21})K} \left(\frac{1}{F} + \frac{1}{F^*} \right), \quad (37)$$

where

$$K = \left(\gamma_{\text{eff}} - i \left\{ \Delta_P - \frac{\epsilon_P}{2\gamma_{\text{eff}} + \gamma_{21}} \left[\left(\frac{1}{F} + \frac{1}{F^*} \right) (-|\Omega_P|^2(\rho_{22} - \rho_{11})^{(0)} + 2\gamma_{31}) \right] \right\} \right. \\ \left. + \frac{|\Omega_C|^2/4}{\gamma_{31} - i(\Delta_P - \Delta_C) + \frac{i\epsilon_P}{2\gamma_{\text{eff}} + \gamma_{21}} \left[\left(\frac{1}{F} + \frac{1}{F^*} \right) (-|\Omega_P|^2(\rho_{22} - \rho_{11})^{(0)} + 2\gamma_{31}) \right]} \right) \quad (38)$$

The analytic closed form results under the weak probe excitation are given above providing the effect of NDD interaction on first- and third-order susceptibilities of probe transitions. However, we focus our attention on the exact results given in the following section.

4. Numerical results

In this section, we will study the steady-state results obtained by numerical integration of Eq. (23) for the dynamical evolution of density matrix elements, EIT and dispersive properties of the λ -type three-level system with NDD interaction included, under different parametric conditions.

4.1. Coherent Population Trapping (CPT) condition

One can achieve CPT condition in the λ -type atomic system when the probe Rabi frequency and coupling Rabi frequency are equal and thus satisfying two-photon resonance condition. We keep $\Omega_P = \Omega_C = 0.5$. All parameters are measured in γ . Initially, $\rho_{11} = 1$, $\rho_{22} = 0$, $\rho_{33} = 0$. Fig. 2(a) displays $\text{Re}(\rho_{12})$ and $\text{Im}(\rho_{12})$ in the steady state as a function of probe detuning Δ_P and keeping $\Delta_C = 0$. The linear susceptibility of probe

transition is proportional to ρ_{12} , with dispersion proportional to $\text{Re}(\rho_{12})$ and absorption proportional to $\text{Im}(\rho_{12})$. Fig. 2(a) shows typical dispersion (solid line), absorption (dash line) curve under CPT condition. The peaks in the absorption curve is due to the dynamic Stark-splitting of the upper level. Fig. 2(b) displays the plot of steady-state values of ρ_{11} , ρ_{22} , ρ_{33} , $\rho_{22} - \rho_{11}$, $\rho_{22} - \rho_{33}$ and $\text{Tr}(\rho)$ as a function of Δ_P , keeping all other parameters same as in Fig. 2(a). The CPT can be clearly observed in the region around $\Delta_P = \Delta_C = 0$, where two-photon resonance condition is satisfied, and $\rho_{22} = 0$ where $\rho_{11} = \rho_{33} = 0.5$. The entire population is trapped in two lower levels and the upper level is empty. The quantities $\rho_{22} - \rho_{11}$ and $\rho_{22} - \rho_{33}$ show dips at $\Delta_P = 0$ with magnitude -0.5 . Also, $\text{Tr} \rho = 1$ for the entire range of Δ_P . The effect of finite positive detuning of coupling field can be seen in Fig. 2(c), where $\Delta_C = 3.5$ has been kept but keeping all other parameters same as in Fig. 2(a). The dip of absorption (dash line) and peak of dispersion move toward $\Delta_P = 3.5$. Both dispersion and absorption curves show their magnitudes zero at $\Delta_P = 3.5$. In Fig. 2(d) the effect of $\Delta_C = 3.5$ can be seen on ρ_{11} , ρ_{22} , ρ_{33} , $\rho_{22} - \rho_{11}$ and $\rho_{22} - \rho_{33}$, while keeping other parameters same as in Fig. 2(b). Here we find that CPT can be observed near $\Delta_P = 3.5$, where $\rho_{22} = 0$ and $\rho_{11} = \rho_{33} = 0.5$. The dips (or peaks) of quantities $\rho_{22} - \rho_{11}$ and $\rho_{22} - \rho_{33}$ move in opposite directions with respect to the point $\Delta_P = 3.5$. The values of these quantities at $\Delta_P = 3.5$ is about -0.5 . The $\text{Tr}(\rho) = 1$ for all values of Δ_P . Figures 2(e) and 2(f) are same as 2(c) and 2(d) but this time $\Delta_C = -3.5$. The profile of dispersion (solid line) curve is upside down and left right inverted when compared to 2(c). The absorption curve (dash line) is left right inverted when compared to 2(c). Both curves have zero magnitude at $\Delta_P = -3.5$. Figure 2(f) is left right inverted from Fig. 2(d). This means CPT is observable when $\Delta_P = -3.5$, i.e., $\rho_{22} = 0$ and $\rho_{11} = \rho_{33} = 0.5$ around $\Delta_P = -3.5$ (satisfying two-photon resonance condition) along with $\rho_{22} - \rho_{11} = \rho_{22} - \rho_{33} = -0.5$. Note $\text{Tr}(\rho) = 1$ throughout.

The effect of NDD interaction is shown in Figs. 3–5. The parameters selected for these figures are same as in Fig. 2 except $\epsilon_P = \epsilon_C = 2.0$; $\gamma_{12}^D = \gamma_{23}^D = 0$ for Figs. 3(a,c) and $\epsilon_P = \epsilon_C = 2.0$; $\gamma_{12}^D = \gamma_{23}^D = 3.0$ for Figs. 3(b,d). Neglecting γ_{12}^D and γ_{23}^D is justified under the limiting condition mentioned after Eq. (12). In Fig. 3(a) two curves represent dispersion (solid line) and absorption (dash line) for the probe transition. When this figure is compared with Fig. 2(a) (where the NDD interaction is zero), there is some noticeable change in absorption i.e., the curve getting flat but the peak in the dispersion curve on the right-hand side is decreased due to non-zero real part of NDD interaction. Similarly, for the diagonal matrix elements of ρ when compared with Fig. 2(b), there is not much change in ρ_{22} due to the real part of NDD interaction but there is asymmetry introduced in ρ_{11} and ρ_{33} due to that. The CPT is observable at $\Delta_P = 0$ ($= \Delta_C$) and at that point $\rho_{11} = \rho_{33} = 0.5$. The peaks of both ρ_{11} and ρ_{33} not occurring at $\Delta_P = 0$. For ρ_{11} it has moved in negative Δ_P region. For ρ_{33} there are two peaks of unequal magnitudes. Also, dips in $\rho_{22} - \rho_{11}$, $\rho_{22} - \rho_{33}$ move in to the opposite directions with reference to $\Delta_P = 0$ (as compared to Fig. 2(b)). Effects of non-zero NDD interaction when its both real and imaginary parts are non-zero is shown in Fig. 3(c) for dispersion (solid line) and absorption (dash line). There are some changes in the widths of absorption/dispersion spectra and magnitudes of curves change when compared with Fig. 2(a). This is due to the enhanced damping introduced by imaginary part of the NDD interaction. The same is true for Fig. 3(d) where some changes are noticeable in

ρ_{11} , ρ_{22} , ρ_{33} . The CPT is observable at $\Delta_P = 0$ ($= \Delta_C$), where $\rho_{11} = \rho_{22} = 0.5$ and asymmetry in ρ_{11} and ρ_{33} curves is still observable with a slight change with respect to Fig. 3(b). The widths of $\rho_{22} - \rho_{11}$, $\rho_{22} - \rho_{33}$ curves also increasing in Fig. 3(d) in comparison to Fig. 3(b).

Next, the effect of non-zero Δ_C along with NDD interaction is displayed in Fig. 4(a,b,c,d), where $\Delta_C = 3.5$ is selected but all other parameters are the same as in Fig. 3. The dip in the absorption curve (dash line) shows going down and up behavior at zero absorption (Fig. 4(a,c)), which is occurring near $\Delta_P = 3.5$, when compared with Fig. 2(c). The dispersion curve also rises sharply when approaching $\Delta_P = 3.5$ (solid curve in Fig. 4(a)) when compared to solid curve in Fig. 2(c). This is due to the non-zero ϵ_P and ϵ_C . The inclusion of non-zero γ_{12}^D and γ_{23}^D causes the dispersion curve to go down in magnitude with increased width of peaks (solid curve in Fig. 4(c)) when compared to solid curve in Fig. 4(a). There are both qualitative and quantitative changes in curves of diagonal matrix elements ρ_{11} , ρ_{22} , ρ_{33} in the presence of NDD interaction and $\Delta_C = 3.5$ as shown in Fig. 4(b). The most noticeable behavior of these curves are near $\Delta_P = 3.5$ where fall of ρ_{11} , and rise of ρ_{33} is quite steep and the dip in ρ_{22} is not smooth. This is all due to the combined effect of $\epsilon_P = \epsilon_C = 2.0$ and $\Delta_C = 3.5$. When $\gamma_{12}^D = \gamma_{23}^D = 3.0$ is included in Fig. 4(d) then magnitudes get diminished. Such behavior are also seen in $\rho_{22} - \rho_{11}$, $\rho_{22} - \rho_{33}$ near $\Delta_P = 3.5$. In Figs. 4(b,d) the CPT is occurring near $\Delta_P = 3.5$ such that $\rho_{22} = 0$, $\rho_{11} = \rho_{33} = 0.5$.

In Fig. 5(a,b,c,d) the value of $\Delta_C = -3.5$ but all other parameters are the same as in Fig. 4(a,b,c,d). The dispersion curve (solid line) when compared to dispersion curve in Fig. 4(a) is now up-side down inverted as well as left-right inverted. The zero dispersion is located at $\Delta = -3.5$. The absorption curve (dash line) in Fig. 5(a) is left-right inverted in comparison to corresponding curve in Fig. 4(a). The zero absorption (dip) occurs at $\Delta = -3.5$. The curve is quite smooth around the dip. In Fig. 5(b) all the diagonal matrix elements are left-right inverted in comparison to corresponding curves in Fig. 4(b). $\rho_{11} = \rho_{33} = 0.5$ at $\Delta_P = -3.5$ and curves are smoothly rising near that point. Also, both $\rho_{22} - \rho_{11}$ and $\rho_{22} - \rho_{33}$ equal to 0.5 at $\Delta_P = -3.5$ with smooth rise near that point in these curves. When imaginary part of the NDD interaction is included Fig. 5(c,d), the magnitude of curves decrease at every point that include peaks and dips when compared to Fig. 4(c,d). This is due to the increased damping caused by the $\gamma^D(s)$.

4.2. Electromagnetically Induced Transparency (EIT) condition

The study of the EIT system under consideration is displayed in Figs. 5–9 with different parametric conditions. In all these studies, the initial condition ($t = 0$) for the density matrix elements has been kept as $\rho_{11}(0) = 1$, $\rho_{22}(0) = \rho_{33}(0) = 0$, and $\rho_{ij}(0) = 0$ $i \neq j$. For Fig. 6(a,b), other parameters are $\Omega_P = 0.1$, $\Omega_C = 5.0$, $\epsilon_P = \epsilon_C = 0$, $\gamma_{21}^D = \gamma_{23}^D = 0$ and all these parameters are measured with respect to γ . The dispersion (solid line) and absorption (dash line) curves are plotted in Fig. 6(a). These curves are typical EIT dispersion-absorption curves [13, 14]. The absorption peaks are situated at $\Delta_P = \pm 2.5$. Both dispersion and absorption curves are at zero magnitude when $\Delta_P = 0$. Under EIT conditions, the population of three levels in the steady state are $\rho_{11} = 1$, $\rho_{22} = 0$, $\rho_{33} = 0$, $\rho_{22} - \rho_{11} = -1$, $\rho_{22} - \rho_{33} = 0$ as shown in Fig. 6(b). Figure 6(a,b) serve as

reference for comparison with Fig. 6(c,d,e,f) when $\Delta_C \neq 0$. Effect of $\Delta_C = 3.5$ is shown in Fig. 6(c,d) in which all other parameters are kept same as in Fig. 6(a,b) but Δ_C is different from zero. The non-zero Δ_C causes asymmetry in absorption/dispersion spectra. Both locations and separation of peaks change. Peaks of absorption are now located at $\Delta_P = 4.8$ and 1.3 consistent with the analysis given in [13, 14]. The zero magnitude of both absorption /dispersion now moves at $\Delta_C = 3.5$. The non-zero Δ_C introduces profile change of both absorption/dispersion curves. The behavior of diagonal matrix elements of ρ and their difference (Fig. 6(d) is the same as Fig. 6(b). When the sign of Δ_C is reversed, i.e., $\Delta_C = -3.5$, then in Fig. 6(e) it can be seen that absorption spectrum is left-right reversed when compared with Fig. 6(c). However the dispersion spectrum in Fig. 6(e) is not only left-right reversed but also upside down when compared with Fig. 6(c). Note that Fig. 6(f) remain same as Fig. 6(b) for the diagonal elements.

In Fig. 7(a,b,c,d) the effect of NDD interaction has been displayed under the EIT conditions. The parameters in Fig. 7(a,b) are the same as in Fig. 6(a,b) except $\epsilon_P = \epsilon_C = 2.0$, i.e., the real part of the NDD interaction is non-zero in Fig. 7(a,b). The profiles of absorption (dash-line) and dispersion (solid-line) curves changed (Fig. 7(a)) compared to Fig. 6(a) and they look similar to the one displayed in Fig. 6(c). The only difference is in the locations of the peaks. In the steady-state, under the EIT conditions $\rho_{11} = 1$, $\rho_{22} = 0$, $\rho_{33} = 0$, $\rho_{22} - \rho_{11} = -1$, $\rho_{22} - \rho_{33} = 0$ as shown in Fig. 7(b). The coefficient ϵ_P comes in the expression as $\epsilon_P(\rho_{22} - \rho_{11})$ and survives in the steady-state but ϵ_C comes in the expression as $\epsilon_C(\rho_{22} - \rho_{33})$ and vanishes in the steady-state. Hence only ϵ_P is retained in the equations of density matrix elements and it behaves like atomic detuning in the steady-state. Fig. 7(b) behaves like Fig. 6(b) more or less meaning $\rho_{11} = 1$, $\rho_{22} = 0$, $\rho_{33} = 0$, $\rho_{22} - \rho_{11} = -1$, $\rho_{22} - \rho_{33} = 0$ in the steady-state. Inclusion of the imaginary part of the NDD interaction $\gamma_{21}^D = \gamma_{23}^D = 3.0$ reduces the peak heights but increases the widths of absorption/dispersion curves in Fig. 7(c) when compared to Fig. 7(a). Clearly, this is due to the enhancement of damping caused by the imaginary part of the NDD interaction. The diagonal elements behavior Fig. 7(d) is the same as the one displayed in Fig. 7(b).

In Fig. 8(a,b) the real part of the NDD interaction as well as other parameters are the same as in Fig. 7(a,b), except $\Delta_C = -3.5$. The effective detuning is the algebraic sum of $\Delta_C = 3.5$ and ϵ_P under steady-state in this situation. Hence the separation of right peaks for both dispersion/absorption curves from $\Delta_P = 0.0$ increases. Also, in Fig. 8(a) the relative separation of two peaks of absorption/dispersion curves also enhances. However, Fig. 8(b) is quite similar to Fig. 7(b) for the diagonal elements. When imaginary part of the NDD interaction is also included by keeping $\gamma_{21}^D = \gamma_{23}^D = 3.0$ (in Fig. 8(b)) and comparison of curves made with Fig. 8(a), the locations of the peaks are unchanged but their widths increase due to the increased damping. The behavior of the diagonal elements (Fig. 8(d)) is same as the one displayed in Fig. 8(b).

Next, the Δ_C is selected as $\Delta_C = -3.5$ in Fig. 9(a,b,c,d) but all other parameters are the same as in Fig. 8(a,b,c,d). By selecting such parameters, the two peaks in the absorption/dispersion curves look identical in shapes and heights and they are symmetrically located around $\Delta_P \approx -2$. The zero absorption and dispersion are also located around the same value of Δ_P . The non-zero ϵ_P and $\Delta_C = -3.5$ combined algebraically and move curves toward $\Delta_P \approx -2$. Fig. 9(b) shows $\rho_{11} = 1$, $\rho_{22} = 0$, $\rho_{33} = 0$, $\rho_{22} - \rho_{11} = -1$,

$\rho_{22} - \rho_{33} = 0$, in the steady-state for all values of Δ_P . When imaginary part of the NDD is also included (Fig. 9(c)), the symmetry, locations, shapes of all curves still maintained as in Fig. 9(a) but the peak heights decrease due to the enhanced damping provided by the imaginary part of the NDD. Note that there is no change in Fig. 9(d) when compared with Fig. 9(b).

5. Conclusion

An ensemble of three-level atoms in λ -type configuration of its levels is considered here. The near dipole-dipole interaction (NDD) for both probe and coupling transitions are included in the density matrix equation of the system. The NDD interactions give rise to a complex coefficient, whose real part provides the frequency shift/detuning and imaginary part introduces an additional radiative damping. The system has been studied under the steady-state condition for both coherent-population-trapping (CPT) and electromagnetically induced transparency (EIT) conditions. In the CPT condition, the lower two-levels are equally populated when $\Delta_P = \Delta_C = 0$ but that changes when Δ_P is non-zero for both $\Delta_C = 0$ and $\Delta_C \neq 0$. There are both qualitative and quantitative changes in absorption/dispersion spectra of the probe transition when NDD interaction is non-zero and $\Delta_C \neq 0$. In the EIT condition, the probe field is kept weak compared to the coupling field, and hence in the steady-state, the entire population stayed in the lower level of the probe transition ($\rho_{11} = 1$). The real part of the NDD interaction provides atomic detuning-like behavior for the probe transition but no effect for the coupling transition. The absorption/dispersion change both qualitatively as well as quantitatively under different values of parameters (specifically for the change of Δ_C and ϵ_P). Inclusion of the imaginary part of the NDD interaction enhances radiative damping and consequently the increase in peak widths and reduction of their amplitudes. These results provide control of absorption/dispersion properties of the three-level system for CPT and EIT phenomena with NDD interactions (in dense atomic medium) and atomic detuning.

Acknowledgments

We thank G. Duree for his encouragement and support for this work.

References

- [1] C. M. Bowden, Near Dipole-Dipole Interaction Effects in Quantum and Nonlinear Optics, in: I. Ramarao (Ed.), Recent Developments in Quantum Optics, Plenum Press, New York, 55–63, 1993.
- [2] C. M. Bowden, A. Postan, R. Inguva, Invariant pulse propagation and self-phase modulation in dense media, *J. Opt. Soc. Am. B* 8 (5) (1991) 1081–1084, doi:10.1364/JOSAB.8.001081.
- [3] C. Stroud, C. Bowden, L. Allen, Self-induced transparency in self-chirped media, *Opt. Commun.* 67 (5) (1988) 387–390, doi:https://doi.org/10.1016/0030-4018(88)90033-8.
- [4] Y. Ben-Aryeh, C. M. Bowden, J. C. Englund, Intrinsic optical bistability in collections of spatially distributed two-level atoms, *Phys. Rev. A* 34 (1986) 3917–3926, doi:10.1103/PhysRevA.34.3917.
- [5] R. Inguva, C. M. Bowden, Spatial and temporal evolution of the first-order phase transition in intrinsic optical bistability, *Phys. Rev. A* 41 (1990) 1670–1676, doi:10.1103/PhysRevA.41.1670.

- [6] Y. Ben-Aryeh, C. Bowden, J. Englund, Longitudinal spacial first-order phase transition in a system of coherently-driven, two-level atoms, *Opt. Commun.* 61 (2) (1987) 147–150, doi: [https://doi.org/10.1016/0030-4018\(87\)90237-9](https://doi.org/10.1016/0030-4018(87)90237-9).
- [7] P. P. Ewald, Zur Begrndung der Kristalloptik, *Annalen der Physik* 354 (1) (1916) 1–38, ISSN 1521-3889, doi:10.1002/andp.19163540102.
- [8] J. P. Dowling, C. M. Bowden, Near dipole-dipole effects in lasing without inversion: An enhancement of gain and absorptionless index of refraction, *Phys. Rev. Lett.* 70 (1993) 1421–1424, doi: 10.1103/PhysRevLett.70.1421.
- [9] A. Joshi, S. V. Lawande, Effects of Dipole Interaction on the Collapse-revival Phenomenon of Rabi Oscillations, *J. Mod. Optic* 38 (7) (1991) 1407–1413, doi:10.1080/09500349114551571.
- [10] A. Joshi, R. R. Puri, S. V. Lawande, Effect of dipole interaction and phase-interrupting collisions on the collapse-and-revival phenomenon in the Jaynes-Cummings model, *Phys. Rev. A* 44 (1991) 2135–2140, doi:10.1103/PhysRevA.44.2135.
- [11] A. Joshi, R. R. Puri, Steady-state behavior of three-level systems in a broadband squeezed bath, *Phys. Rev. A* 45 (1992) 2025–2030, doi:10.1103/PhysRevA.45.2025.
- [12] H. Wang, D. J. Goorskey, M. Xiao, Atomic coherence induced Kerr nonlinearity enhancement in Rb vapour, *Journal of Modern Optics* 49 (3-4) (2002) 335–347, doi:10.1080/09500340110089938.
- [13] J. P. Marangos, Electromagnetically induced transparency, *Journal of Modern Optics* 45 (3) (1998) 471–503, doi:10.1080/09500349808231909.
- [14] M. Fleischhauer, A. Imamoglu, J. P. Marangos, Electromagnetically induced transparency: Optics in coherent media, *Rev. Mod. Phys.* 77 (2005) 633–673, doi:10.1103/RevModPhys.77.633.

Figure Captions

Figure 1: Diagram of the three-level system in a Λ -configuration of its levels, driven by probe and coupling lasers of frequencies ω_P and ω_C , respectively.

Figure 2: Plots of density matrix elements as a function of the probe detuning Δ_P without NDD interaction under parametric conditions $\Omega_P = \Omega_C = 5.0$ (CPT condition), $\epsilon_P = \epsilon_C = 0$, and $\gamma_{21}^D = \gamma_{23}^D = 0$. All parameters are measured with respect to γ . Plots (a), (c), and (e) are for the real and imaginary parts of ρ_{12} , which are proportional to the real and imaginary parts of the first order susceptibility of the probe transition when $\Delta_C = 0, 3.5$, and -3.5 , respectively. Plots (b), (d), and (f) show ρ_{11} , ρ_{22} , ρ_{33} , $\rho_{22} - \rho_{11}$, $\rho_{22} - \rho_{33}$, and $\text{Tr}(\rho)$ when $\Delta_C = 0, 3.5$, and -3.5 , respectively.

Figure 3: Plots of density matrix elements as a function of the probe detuning Δ_P with NDD interaction under parametric conditions $\Omega_P = \Omega_C = 5.0$ (CPT condition), $\epsilon_P = \epsilon_C = 2.0$, and $\Delta_C = 0$. All parameters are measured with respect to γ . Plots (a) and (c) are for the real and imaginary parts of ρ_{12} , which are proportional to the real and imaginary parts of the first order susceptibility of the probe transition when $\gamma_{21}^D = \gamma_{23}^D = 0$ and 3.0 , respectively. Plots (b) and (d) show ρ_{11} , ρ_{22} , ρ_{33} , $\rho_{22} - \rho_{11}$, $\rho_{22} - \rho_{33}$, and $\text{Tr}(\rho)$ when $\gamma_{21}^D = \gamma_{23}^D = 0$ and 3.0 , respectively.

Figure 4: Same as Fig. 3 but with $\Delta_C = 3.5$.

Figure 5: Same as Fig. 3 but with $\Delta_C = -3.5$.

Figure 6: Plots of density matrix elements as a function of the probe detuning Δ_P without NDD interaction under parametric conditions $\Omega_P = 0.1, \Omega_C = 5.0$ (EIT condition), $\epsilon_P = \epsilon_C = 0$, and $\gamma_{21}^D = \gamma_{23}^D = 0$. All parameters are measured with respect to γ . Plots (a), (c), and (e) are for the real and imaginary parts of ρ_{12} , which are proportional to the real and imaginary parts of the first order susceptibility of the probe transition when $\Delta_C = 0, 3.5$, and -3.5 , respectively. Plots (b), (d), and (f) show ρ_{11} , ρ_{22} , ρ_{33} , $\rho_{22} - \rho_{11}$, $\rho_{22} - \rho_{33}$, and $\text{Tr}(\rho)$ when $\Delta_C = 0, 3.5$, and -3.5 , respectively.

Figure 7: Plots of density matrix elements as a function of the probe detuning Δ_P with NDD interaction under parametric conditions $\Omega_P = 0.1, \Omega_C = 5.0$ (EIT condition), $\epsilon_P = \epsilon_C = 2.0$, and $\Delta_C = 0$. All parameters are measured with respect to γ . Plots (a) and (c) are for the real and imaginary parts of ρ_{12} , which are proportional to the real and imaginary parts of the first order susceptibility of the probe transition when $\gamma_{21}^D = \gamma_{23}^D = 0$ and 3.0 , respectively. Plots (b) and (d) show ρ_{11} , ρ_{22} , ρ_{33} , $\rho_{22} - \rho_{11}$, $\rho_{22} - \rho_{33}$, and $\text{Tr}(\rho)$ when $\gamma_{21}^D = \gamma_{23}^D = 0$ and 3.0 , respectively.

Figure 8: Same as Fig. 7 but with $\Delta_C = 3.5$.

Figure 9: Same as Fig. 7 but with $\Delta_C = -3.5$.

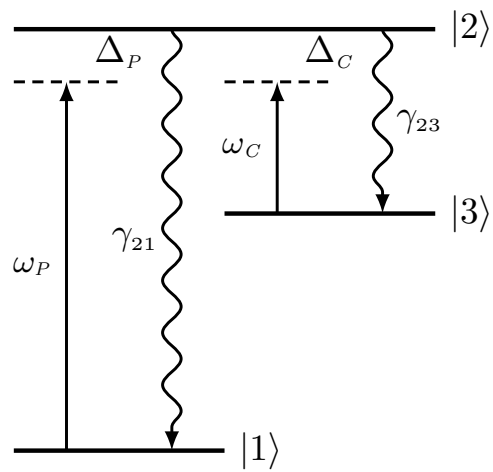


Figure 1: Diagram of the three-level system in a Λ -configuration and driven by a probe and coupling lasers of frequencies ω_P and ω_C , respectively.

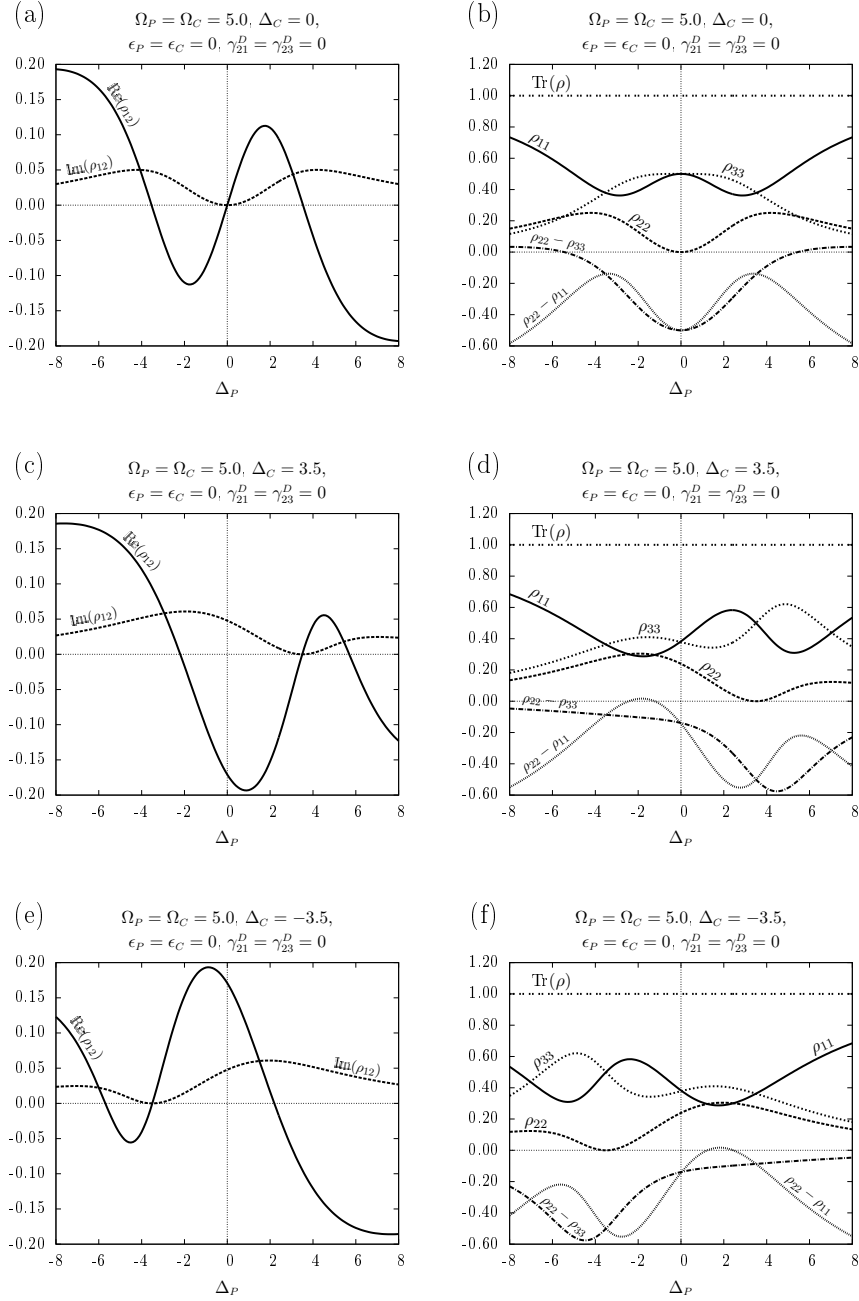


Figure 2:

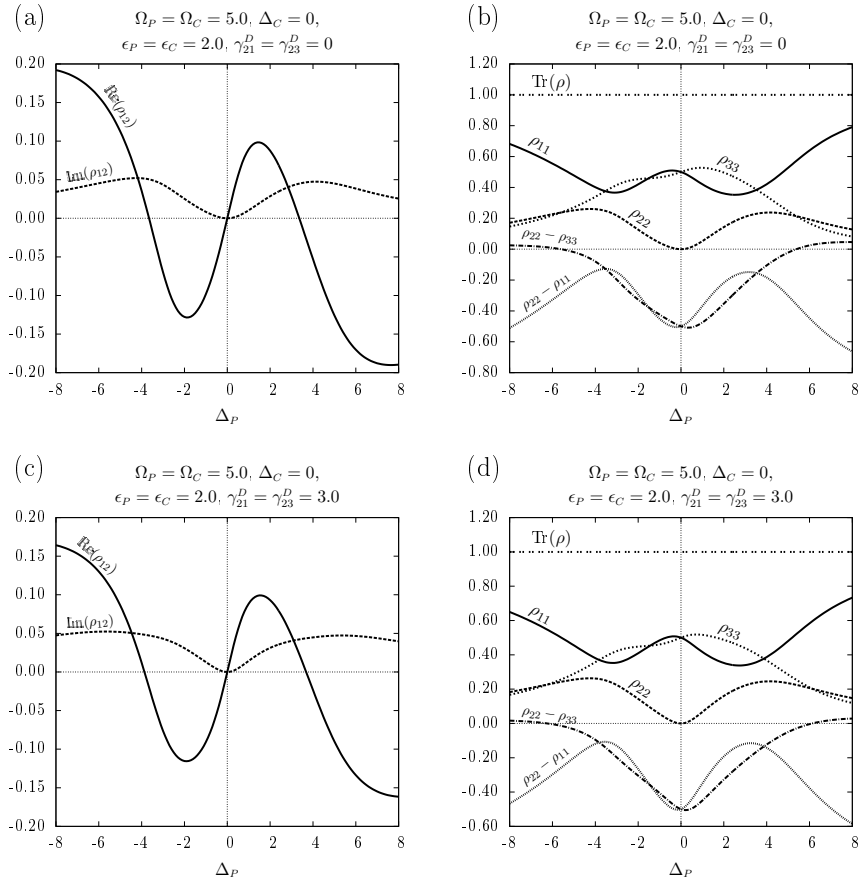


Figure 3:

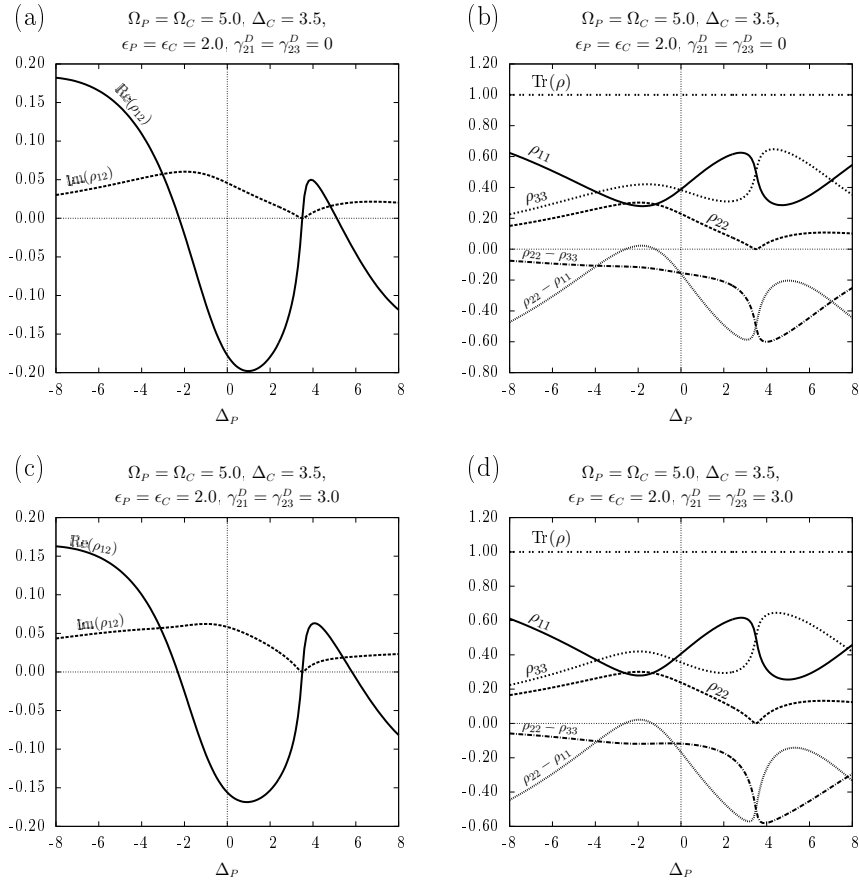


Figure 4:

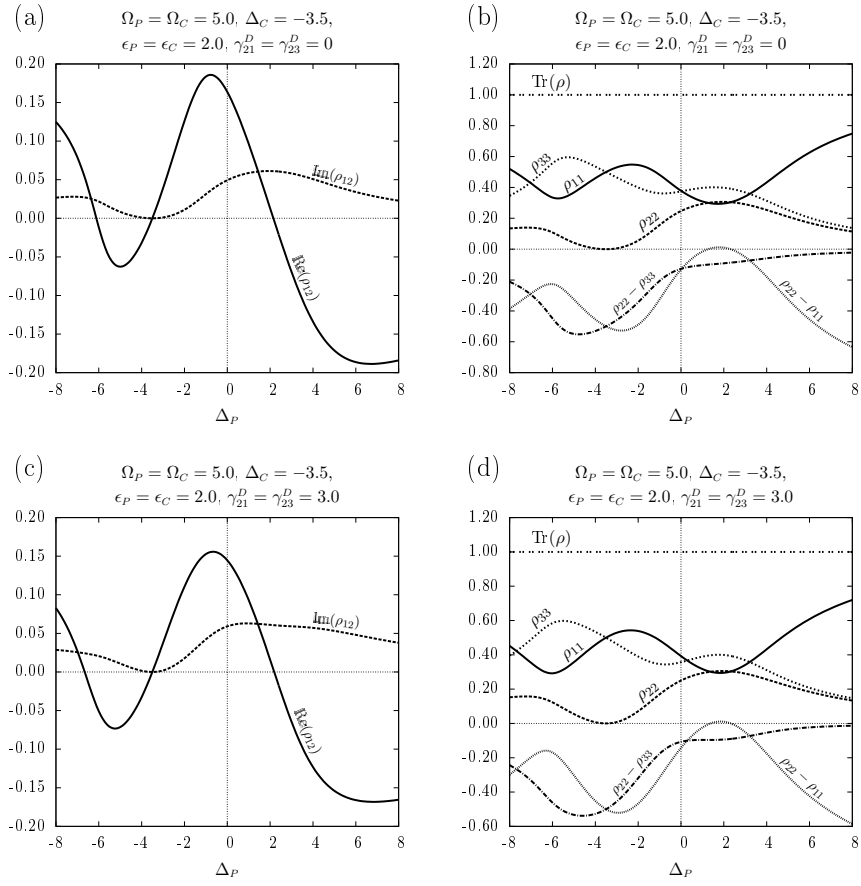


Figure 5:

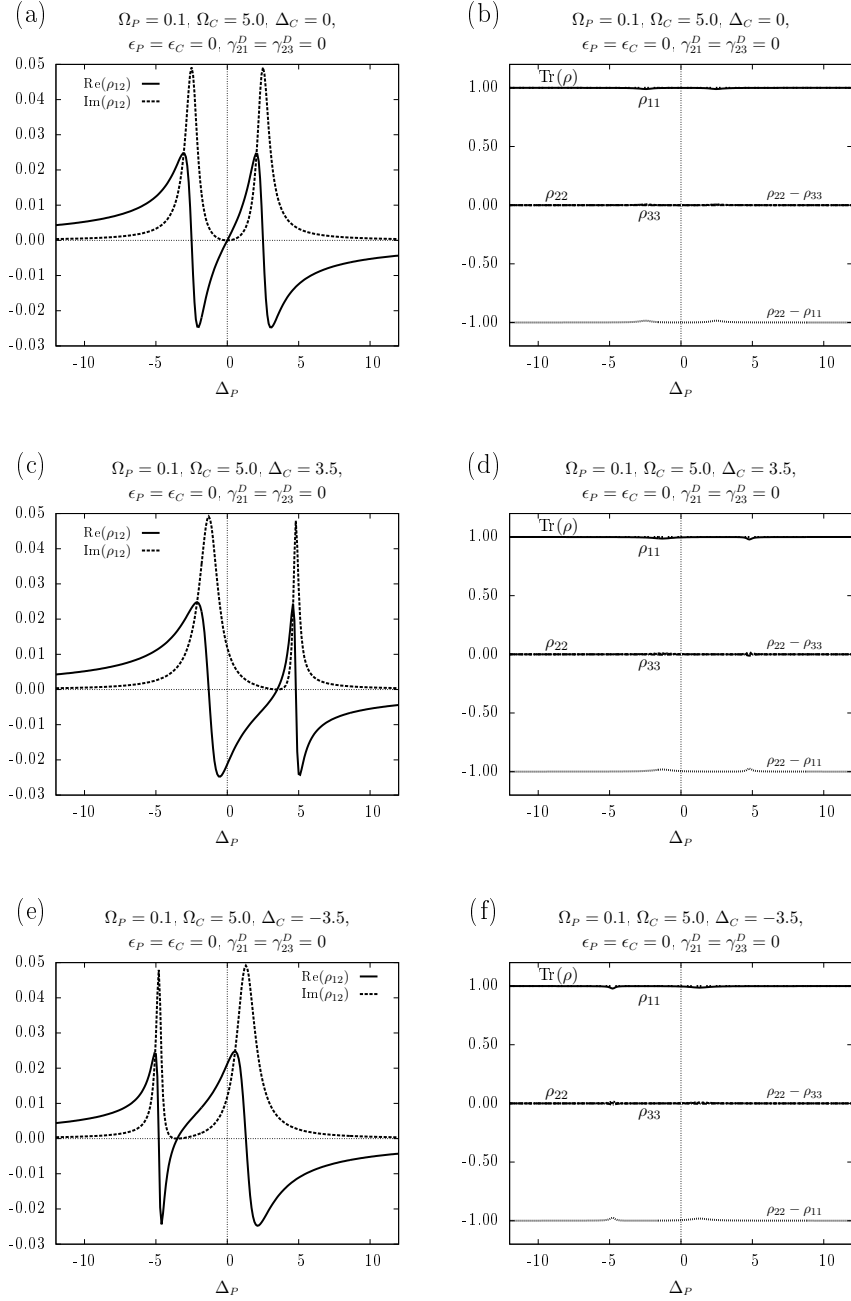


Figure 6:

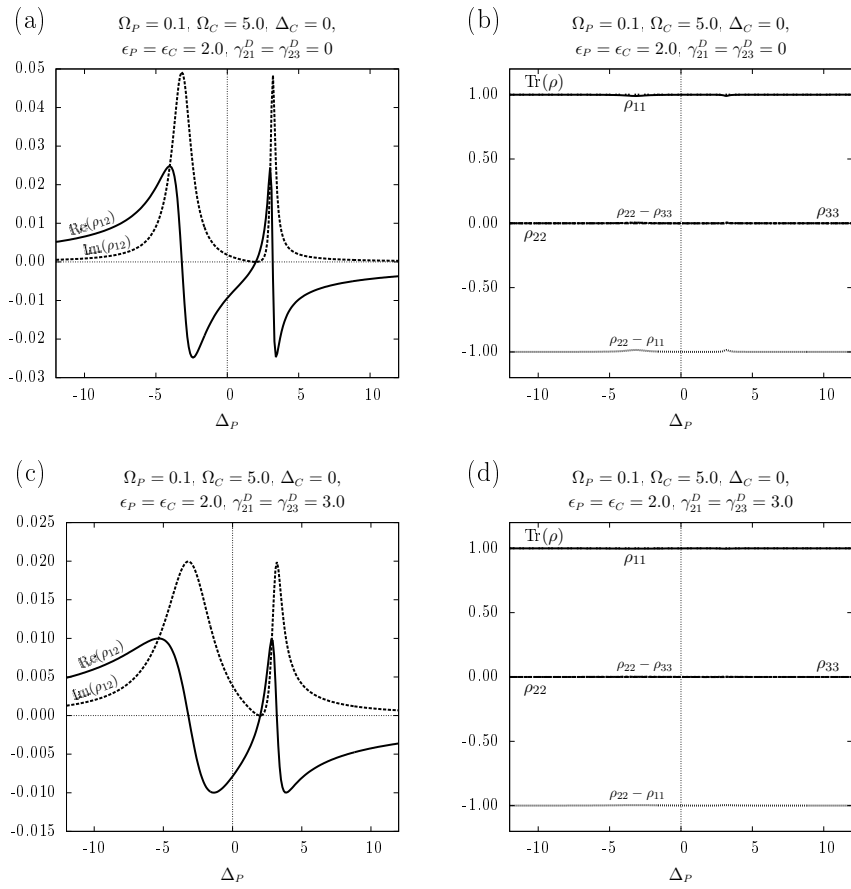


Figure 7:

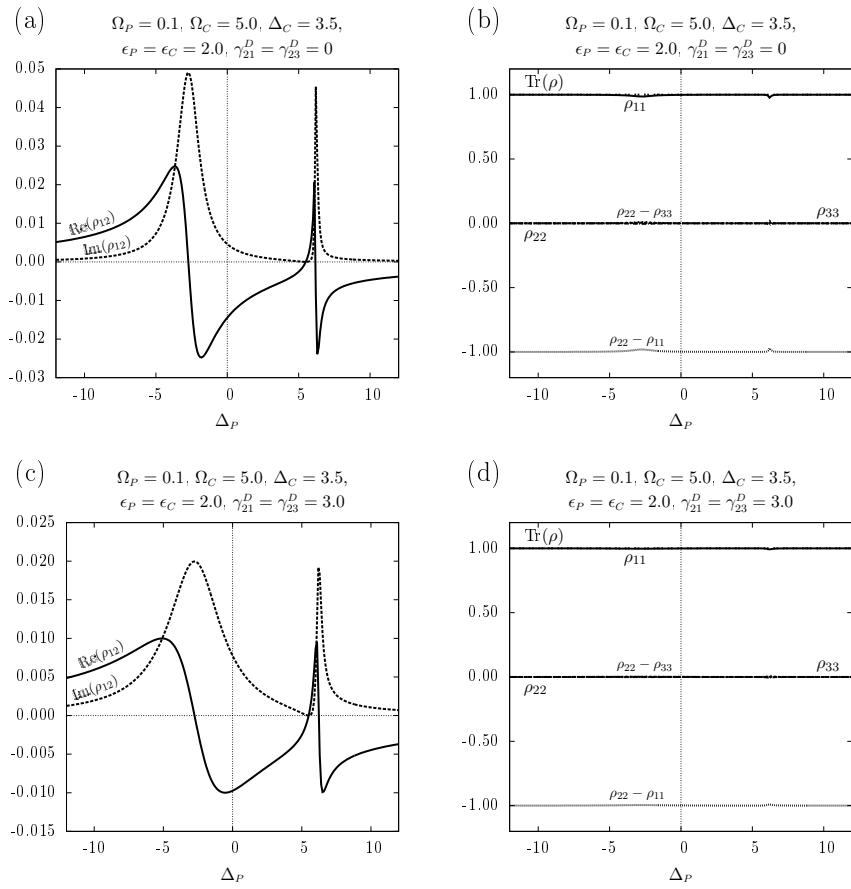


Figure 8:

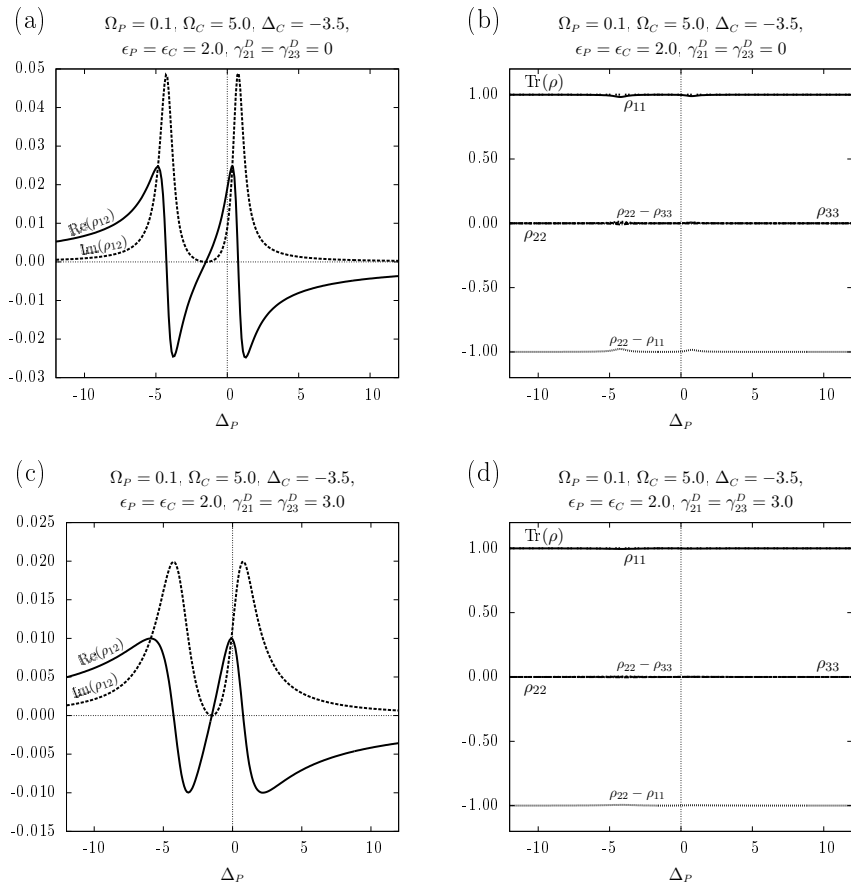


Figure 9: